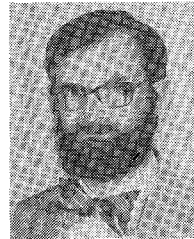


which is different for different values of  $R_T$ . In making measurements with large values of  $R_T$  it was necessary to insure that  $C_B$ ,  $C_C$ , and other stray capacitances did not significantly load the test transistor base circuit at the modulation frequency. Also, it was necessary to locate the RFC's and  $C_B$  carefully to insure that microwave power did not enter the response measurement instrumentation. It was also found that in some RF generation equipment, the modulation scheme may introduce a video component on the RF line which, if not properly grounded through a dc path in the stub tuners, and otherwise decoupled through  $C_C$ , could be mistaken for test device response.

## REFERENCES

- [1] R. E. Richardson, V. G. Puglielli, and R. A. Amadori, "Microwave interference effect in bipolar transistors," *IEEE Trans. Electromagn. Compat.*, vol. EMC-17, pp. 216-219, Nov. 1975.
- [2] R. E. Richardson, "Modeling of microwave rectification RFI effects in low frequency circuitry," in *Proc. IEEE Int. Symp. Electromagn. Compat.*, Atlanta, GA, June 20-22, 1978.
- [3] M. L. Forcier and R. E. Richardson, "Microwave rectification RFI response in field effect transistors," *IEEE Trans. Electromagn. Compat.*, vol. EMC-21, pp. 312-315, Nov. 1979.
- [4] H. C. Torrey and C. A. Whitmer, *Crystal Rectifiers*. Lexington, MA: Boston Technical, 1964.
- [5] R. L. Pritchard, "Two dimensional current flow in junction transistors at high frequencies," *Proc. IRE*, vol. 46, pp. 1152-1160, June 1958.

- [6] H. Nath Ghosh, "A distributed model of the junction transistor and its application in the prediction of the emitter base diode characteristic, base impedance, and pulse response of the device," *IEEE Trans. Electron Devices*, vol. ED-12, pp. 513-531, Oct. 1965.
- [7] P. E. Gray and C. L. Searle, *Electronic Principles, Physics Models and Circuits*. New York: Wiley, 1969, ch. 12.
- [8] R. C. Kumar, D. J. Roulston, and S. S. Chamberlain, "A study of the effect of peripheral injection in bipolar transistors using simplified computer analysis," *IEEE Trans. Electron Devices*, vol. ED-24, pp. 86-91, Feb. 1977.
- [9] N. G. Chamberlain and D. J. Roulston, "Modeling of emitter-base bulk and space-charge-layer recombination currents in bipolar transistors," *IEEE Trans. Electron Devices*, vol. ED-23, pp. 1345-1346, Dec. 1976.
- [10] G. Rey, "Effets de la defocalisation (cc et ca) sur le comportement des transistors a jonctions," in *Solid State Electronics*, vol. 12. New York: Pergamon, 1969, pp. 645-659.



Robert E. Richardson, Jr. was born in Bridgeport, CT, on February 26, 1942. He received the B.S.E.E. degree from the University of New Hampshire, Durham, in 1965, and the M.S.E.E. and Ph.D. degrees in electrical engineering from Worcester Polytechnic Institute (WPI), Worcester, MA, in 1971.

While at WPI he was employed at the WPI open pool Nuclear Reactor Facility. In 1972 he joined the technical staff at the Naval Surface Weapons Center, Dahlgren, VA, where he is conducting research on electromagnetic compatibility problems.

Dr. Richardson is a member of Tau Beta Pi.

## Integrated $\Lambda$ -Type Differential Negative Resistance MOSFET Device

CHING-YUAN WU, MEMBER, IEEE, AND KHUN-NAN LAI, STUDENT MEMBER, IEEE

**Abstract**—A new type of the NELS (*n*-channel enhancement mode with load operated at saturation)-connected  $\Lambda$ -type differential negative resistance MOSFET, using the merged integrated circuit of a NELS inverter and an *n*-channel enhancement MOS driver, is studied both experimentally and theoretically. The principal operation of the lambda MOSFET device is characterized by the simple circuit model and device physics. The important device properties, such as the peak voltage, the peak current, the valley voltage, and the negative resistance, are derived in terms of the known device parameters. Comparisons between characteristics of the fabricated device and the theoretical model are made, which show the theoretical analyses are in good agreement with the observed device characteristics.

Manuscript received December 8, 1978; revised June 22, 1979. This research was supported by the National Sciences Council, Republic of China, under Contract NSC-65E-0404-04(01).

The authors are with the Institute of Electronics, National Chiao Tung University, Hsinchu, Taiwan, Republic of China.

## LIST OF SYMBOLS

$C_0$	Gate oxide capacitance per unit area.
$G_0$	Drain-to-source conductance with zero drain voltage.
$G_{01}$	$G_0$ of transistor $Q_1$ for the NELS-connected structure.
$G_{02}$	$G_0$ of transistor $Q_2$ for the NELS-connected structure.
$G_{03}$	$G_0$ of transistor $Q_3$ for the NELS-connected structure.
$G_r$	Ratio of $G_{02}$ and $G_{01}$ .
$I_{DS}$	Drain-source current.
$I_p$	Peak current.
$I_v$	Valley current.
$K$	Modifying substrate factor.
$L$	Channel length.
$N_A$	Doping concentration of p-type substrate.
$Q_{ss}$	Surface state charge density.
$Q_B$	Surface depletion layer charge density.

$q$	Electronic charge.
$R_N$	Negative differential resistance.
$V_{DS}$	Drain-source bias voltage.
$V_{FB}$	Flat-band voltage of MOS capacitor.
$V_{GS}$	Gate-source bias voltage.
$V_{GG}$	Applied gate voltage for the NELS-connected structure.
$V_p$	Peak voltage.
$V_T$	Threshold voltage.
$V_V$	Valley voltage.
$Z$	Channel width.
$\phi_{fp}$	The potential difference between Fermi-potential and the intrinsic potential of p-type substrates at the flat-band condition.
$\phi_{MS}$	Metal-semiconductor work function difference.
$\epsilon_s$	Dielectric permittivity of silicon substrate.
$\mu_n$	Surface mobility of the electron.
$\mu_{FE}$	Field effect mobility.

## I. INTRODUCTION

RECENTLY, several types of voltage-controlled negative differential resistance devices with the integrated transistor structure have been reported [1]–[6]. Among these, Takagi and Kano [1] reported a structure of two complementary junction field effect transistors with two terminals, which involved rather complicated integrated circuit fabrication technology. Other structures [2]–[6] were reported which had three terminals, but were shown to have some disadvantages; namely, the combination of JFET and the bipolar transistor with a different carrier type [5], [6], the difficulty in controlling the negative resistance region [2], [4], [5], and a rather large valley current [3], [5].

A new type of voltage-controlled negative resistance device—lambda MOSFET, which has three terminals, has been developed [7]. It has been shown that the lambda MOSFET not only involves very simple existing MOS integrated circuit fabrication technology but also exhibits controllable and useful characteristics. An analytical model of the NELS-connected  $\Lambda$ -type differential negative resistance MOSFET will be presented in Section II where the important device properties, such as the peak voltage, the valley voltage, and negative resistance, are derived in terms of the known device parameters. Comparisons between the characteristics of the fabricated devices and the theoretical model will be given in Section III where the theoretical analysis is shown to be in good agreement with the observed device characteristics. In the last section, conclusions will be made.

## II. DEVICE OPERATION AND SECTIONAL MODELS

The basic circuit representation of the NELS-connected  $\Lambda$ -type MOSFET is shown in Fig. 1, which consists of three n-channel enhancement mode MOSFET's with a NELS-MOS inverter and an NMOS driver. Transistor  $Q_1$  acts as a load resistor with the gate shorted to the drain, which is used to modulate the input gate voltage of transistor  $Q_3$ , and transistor  $Q_2$  behaves as an active switch with the gate electrode connected to the drain electrode of the driver transistor  $Q_3$ . The substrate of the load transistor  $Q_1$ , and the substrate and the source of transistors  $Q_2$  and  $Q_3$ , are connected together.

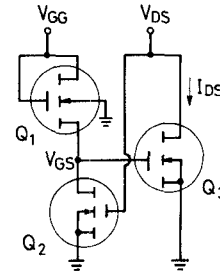


Fig. 1. A NELS-connected  $\Lambda$ -type negative resistance structure.

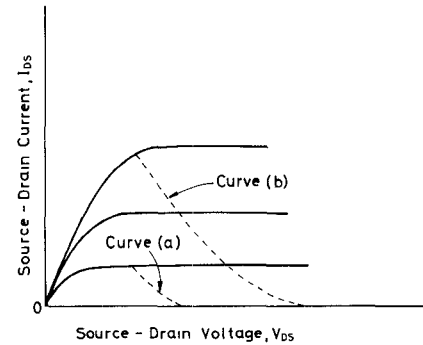


Fig. 2. Two possible cases with the negative differential resistance effect for a MOSFET driver.

There are two possible modes of operation of transistor  $Q_3$  which demonstrate differential negative resistance, as shown in Fig. 2. Curve (a) illustrates the case in which the peak current occurs in the saturation region of  $Q_3$  and curve (b) illustrates the case in which the peak current occurs in the linear region.

Under the conventional assumptions of gradual channel approximation being valid, channel-length modulation effect being negligible, and electron mobility being constant, the current equation for an n-channel MOSFET operating in the linear region can be written as

$$I_{DS} = G_0 \left\{ \left[ V_{GS} - V_{FB} - 2\phi_{fp} - \frac{V_{DS}}{2} \right] V_{DS} - \frac{2}{3} K [(V_{DS} + 2\phi_{fp})^{3/2} - (2\phi_{fp})^{3/2}] \right\} \quad (1)$$

where

$$G_0 = \frac{\mu_n Z C_0}{L}, \quad K = \frac{(2\epsilon_s q N_A)^{1/2}}{C_0}.$$

In order to obtain analytical expressions, the back gate bias effect is assumed to be negligible. This assumption leads to simplified expressions as follows:

$$I_{DS} = G_0 \left\{ [V_{GS} - V_T] V_{DS} - \frac{V_{DS}^2}{2} \right\}, \quad \text{for the linear region} \quad (2)$$

$$I_{DS} = \frac{G_0}{2} [V_{GS} - V_T]^2, \quad \text{for the saturation region} \quad (3)$$

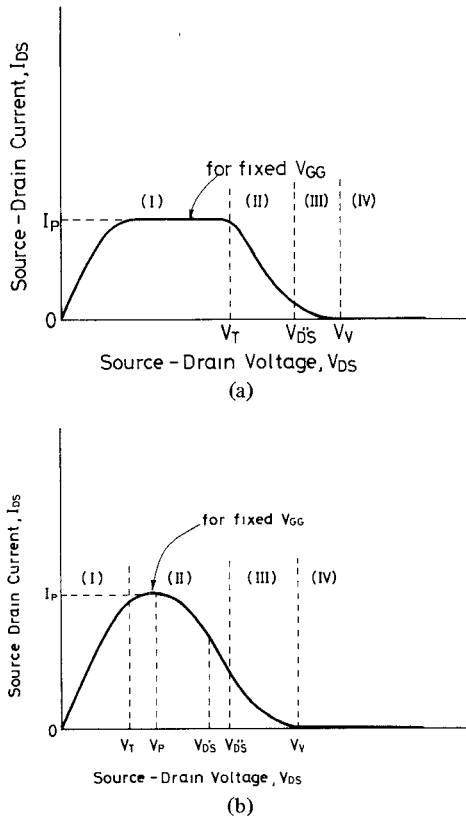


Fig. 3. Three section model for the analysis of a  $\Lambda$ -type negative resistance structure with  $V_p$ . (a) In the saturation region. (b) In the linear region.

where threshold voltage  $V_T$  and the drain-to-source conductance at zero drain voltage  $G_0$  are two important parameters in the analysis. Conventionally, the threshold voltage of the n-channel MOSFET is defined as

$$V_T = \phi_{MS} - \frac{Q_{SS}}{C_0} + 2\phi_{fp} - \frac{Q_B}{C_0}$$

and the ratio of the drain-to-source conductance at zero drain voltage for  $Q_2$  to that of  $Q_1$  is expressed as

$$G_r = G_{02}/G_{01}. \quad (4)$$

For simplifying the analysis, the output characteristic of the NELS-connected MOSFET device is divided into four regions as shown in Fig. 3(a) and (b), which are analyzed separately as follows.

#### Region I

In this region, transistor  $Q_2$  is off and transistor  $Q_1$  is kept in saturation. In order to sustain sufficient voltage across the drain to source of transistor  $Q_1$  and maintain the channel nearly on, the gate-to-source voltage  $V_{GS}$  of Fig. 1 can be expressed as

$$V_{GS} = V_{GG} - V_T - K[\sqrt{2\phi_{fp} + V_{GS}} - \sqrt{2\phi_{fp}}] \quad 0 \leq V_{DS} < V_T \quad (5)$$

where the third term on the right-hand side is the threshold voltage change due to the substrate bias effect of transistor  $Q_1$ .

Solving (5) for  $V_{GS}$  gives

$$V_{GS} = \left( V_{GG} - V_T + K\sqrt{2\phi_{fp}} + \frac{K^2}{2} \right) + K \left[ V_{GG} - V_T + K\sqrt{2\phi_{fp}} + \frac{K^2}{4} + 2\phi_{fp} \right]^{1/2}. \quad (6)$$

Equation (6) shows that  $V_{GS}$  is a function of  $V_{GG}$  and is independent of  $V_{DS}$ . The output current  $I_{DS}$  depends upon whether transistor  $Q_3$  is operated in the linear region or in the saturation region. These conditions are classified as follows.

For  $V_{DS}$  of  $Q_3$  in the range  $V_{DS} \geq V_{GS} - V_T$ ,  $Q_3$  is in saturation, and the drain current is given by

$$I_{DS} = \frac{G_{03}}{2} (V_{GS} - V_T)^2 \quad (7)$$

where  $V_{GS}$  is given by (6).

For  $V_{DS}$  of  $Q_3$  in the range  $V_{DS} < V_{GS} - V_T$ ,  $Q_3$  is in the linear region, and the drain current is given by

$$I_{DS} = G_{03} [(V_{GS} - V_T)V_{DS} - \frac{1}{2} V_{DS}^2]. \quad (8)$$

Two different cases can now occur.

*Case I-a:*  $Q_3$  goes into saturation while in Region I [Fig. 3(a)].

*Case I-b:*  $Q_3$  remains in the linear region throughout Region I [Fig. 3(b)].

#### Region II

In this region,  $V_{DS}$  exceeds the threshold voltage of  $Q_2$ , and the drain voltage is such that transistor  $Q_2$  remains in saturation. Since transistor  $Q_1$  is always kept in saturation, we have

$$V_{DS} - V_T = \frac{1}{\sqrt{G_r}} [(V_{GG} - V_T) - K(\sqrt{2\phi_{fp} + V_{GS}} - \sqrt{2\phi_{fp}}) - V_{GS}] \quad \text{for } V_T \leq V_{DS} \leq V_{GS} + V_T. \quad (9)$$

Operation in this region may also be classified into two cases.

*Case II-a:* Transistor  $Q_3$  remains in saturation throughout Region II [Fig. 3(a)] when transistor  $Q_3$  is operated in the saturation region; (7) gives the current where  $V_{GS}$  is obtained from (9).

*Case II-b:*  $Q_3$  starts out in Region II in the linear region, and goes into saturation at  $V'_{DS}$  [Fig. 3(b)].

When transistor  $Q_3$  is in the linear region, (8) applies. This case always occurs for large values of  $V_{GG}$ .

The breakpoint  $V'_{DS}$  between Case II-a and Case II-b as shown in Fig. 3(b) is derived by substituting  $V_{GS} = V_{DS} + V_T$  into (9); i.e.,

$$V'_{DS} = [2(G_r^{1/2} + 1)(V_{GG} + K\sqrt{2\phi_{fp}} - 2V_T) + K^2] / \{ 2(G_r^{1/2} + 1)^2 + [4K^2(G_r^{1/2} + 1) \cdot (V_{GG} + K\sqrt{2\phi_{fp}} - 2V_T) + K^4 - 4K^2(G_r^{1/2} + 1) \times (2\phi_{fp} + V_T)]^{1/2} \} / 2(G_r^{1/2} + 1)^2. \quad (10)$$

TABLE I  
THE OPERATING POINTS OF EACH TRANSISTOR FOR A NELS  
LAMBDA MOSFET

	Q <sub>1</sub>	Q <sub>2</sub>	Q <sub>3</sub>
Region I	SAT	OFF	LIN → SAT (Case Ia) LIN (Case Ib)
Region II	SAT	SAT	SAT (Case IIa) LIN → SAT (Case IIb)
Region III	SAT	LIN	SAT
Region IV	SAT	LIN	OFF

### Region III

In this region, Q<sub>2</sub> is in the linear region. From Fig. 3(a) and (b), the breakpoint  $V_{DS}''$  between Region II and Region III can be found by substituting  $V_{GS} = V_{DS} - V_T$  into (9), to obtain

$$V_{DS}'' = [2(G_r^{1/2} + 1)(V_{GG} + K\sqrt{2\phi_{fp}}) + K^2]/2(G_r^{1/2} + 1)^2 \\ + \{[4K^2(G_r^{1/2} + 1)(V_{GG} + K\sqrt{2\phi_{fp}})K^4 - 4K^2(G_r^{1/2} + 1) \\ \times (2\phi_{fp} - V_T)]^{1/2}\}/2(G_r^{1/2} + 1)^2. \quad (11)$$

From the equality between the drain currents of Q<sub>1</sub> and Q<sub>2</sub>, a transfer relation can be written as

$$V_{DS} - V_T = \frac{1}{2} \{V_{GS} + [(V_{GG} - V_T) - V_{GS} \\ - K\sqrt{2\phi_{fp} + V_{GS}} - \sqrt{2\phi_{fp}}]^2/(G_r V_{GS})\} \\ \text{for } V_{DS} \geq V_{GS} + V_T. \quad (12)$$

Since transistor Q<sub>3</sub> is operated in saturation region; i.e., for  $V_T \leq V_{GS} \leq V_{DS} + V_T$ , we have

$$I_{DS} = \frac{G_{03}}{2} [V_{GS} - V_T]^2 \quad (13)$$

where  $V_{GS}$  can be found from (12).

### Region IV

In this case, transistor Q<sub>3</sub> is off for  $0 \leq V_{GS} < V_T$ , so we obtain

$$I_{DS} = 0. \quad (14)$$

In order to clarify these four regions the operating points of each transistor are shown in Table I.

### III. THE DETERMINATION OF DEVICE DC PARAMETERS

In order to accurately determine the device dc parameters, the mobility variation with respect to the gate voltage should be considered. In general, the drain-to-source conductance at zero drain voltage  $G_{03}$  can be expressed by

$$G_{03} = A(V_{GS} - V_T)^{-r} \quad (15)$$

where  $A$  and  $r$  are two positive real constants.

From the considerations in Section II, the peak voltage and the peak current for the case shown in Fig. 3(a) can be expressed by

$$V_p = V_T \quad (16)$$

$$I_p = \frac{A}{2} (V_{GS} - V_T)^{2-r} \quad (17)$$

where  $V_{GS}$  is expressed by (6).

Unfortunately, it is difficult to find the peak voltage and the peak current for the case shown in Fig. 3(b) in the analytical form. An alternative method is proposed to calculate  $V_p$  and  $I_p$  by solving the following simultaneous equations, which are

$$V_{DS} = V_T + \frac{1}{G_r^{1/2}} [(V_{GG} - V_T) \\ - K(\sqrt{2\phi_{fp} + V_{GS}} - \sqrt{2\phi_{fp}}) - V_{GS}] \\ \text{for } V_T \leq V_{DS} \leq V_{GS} + V_T \quad (18)$$

$$I_{DS} = A(V_{GS} - V_T)^{1-r} V_{DS} - \frac{A}{2} (V_{GS} - V_T)^{-r} V_{DS}^2 \\ \text{for } V_{DS} + V_T \leq V_{GS}. \quad (19)$$

The valley voltage  $V_v$  of the output characteristic is found at the time when transistor Q<sub>3</sub> is off. This can be obtained by substituting  $V_{GS} = V_T$  into (12); i.e.,

$$V_v = \frac{3}{2} V_T + \frac{[(V_{GG} - 2V_T) - K(\sqrt{2\phi_{fp} + V_T} - \sqrt{2\phi_{fp}})]^2}{2G_r V_T}. \quad (20)$$

Theoretically, the valley current is assumed to be zero, but the thermal leakage current cannot be neglected for MOSFET; thus, we obtain

$$I_V = I_{DSS} \text{ (leakage)}. \quad (21)$$

In general, the typical value of the leakage current for MOSFET is about several tenths of a nanoampere.

The value of the negative differential resistance is defined as

$$R_N = \left. \frac{\partial V_{DS}}{\partial I_{DS}} \right|_{V_{GG} = \text{constant}}. \quad (22)$$

For Region II, the calculation of negative resistance must be classified into two cases which are cited in Fig. 3(a) and (b). For the case of Fig. 3(a), we have

$$R_N = \left. \frac{\partial V_{DS}}{\partial I_{DS}} \right|_{V_{GG} = \text{constant}} \\ = \left( \frac{\partial V_{DS}}{\partial V_{GS}} \right) \left( \frac{\partial V_{GS}}{\partial I_{DS}} \right) \Big|_{V_{GG} = \text{constant}} \\ = \frac{-[K(2\phi_{fp} + V_{GS})^{-1/2} + 2]}{AG_r^{1/2}(2-r)(V_{GS} - V_T)^{1-r}} \\ \text{for } V_T < V_{DS} \leq V_{DS}'' \quad (23)$$

where  $V_{DS}''$  is the breakpoint of Regions II and III, as shown in (11), and  $V_{GS}$  can be found from (9).

From Fig. 3(b), we also calculate the negative resistance in the range  $V_p < V_{DS} \leq V_{DS}'$ , where  $V_p$  is the peak voltage obtained from the simultaneous solution of (18) and (19); thus, we have

$$R_N = \{-[K(2\phi_{fp} + V_{GS})^{-1/2} + 2]\} / \{-A(V_{GS} - V_T)^{1-r} \\ \times \{[K(2\phi_{fp} + V_{GS})^{-1/2} + 2] \\ + 2A(1-r)G_r^{1/2}(V_{GS} - V_T)^{-r}f(V_{GS}) \\ + A(V_{GS} - V_T)^{-r}[K(2\phi_{fp} + V_{GS})^{-1/2} + 2]f(V_{GS}) \\ + rAG_r^{1/2}(V_{GS} - V_T)^{1-r}f^2(V_{GS})\} \quad (24)$$

where

$$f(V_{GS}) = V_T + \frac{1}{G_r^{1/2}} \\ \cdot [(V_{GG} - V_T) - K(\sqrt{2\phi_{fp} + V_{GS}} - \sqrt{2\phi_{fp}}) - V_{GS}]$$

and  $V_{GS}$  can be calculated from (9).

For Region III, by virtue of (12), the negative resistance is

$$R_N = \{-[K(2\phi_{fp} + V_{GS})^{-1/2} + 2] V_{GS} g(V_{GS}) \\ - g^2(V_{GS}) + G_r V_{GS}^2\} / \{(2-r)AG_r(V_{GS} - V_T)^{3-r}\} \\ \text{for } V_{DS}'' \leq V_{DS} < V_v \quad (25)$$

where

$$g(V_{GS}) = [(V_{GG} - V_T) - K(\sqrt{2\phi_{fp} + V_{GS}} - \sqrt{2\phi_{fp}}) - V_{GS}]$$

and  $V_v$  is the valley voltage expressed in (20), and  $V_{GS}$  can be calculated from (12).

#### IV. EXPERIMENTAL RESULTS AND THEORETICAL COMPARISONS

From Fig. 3 and the calculated results of Section III, transistors  $Q1$  and  $Q2$  play an important role in the control of the negative resistance range. For the purpose of high current operation, the layout dimension of transistor  $Q3$  is the main factor. Moreover, the inversion layer effective mobility and substrate doping concentration should be responsible for the characteristic of the device.

Generally, the testing device used for the analysis is designed with  $G_r \neq 1$ . The layout parameters of the testing device are shown in Table II, where the geometric and effective dimensions are listed. The metallization pattern of the fabrication mask of the integrated device is shown in Fig. 4. The typical output characteristic of the fabricated Al-gate  $\Lambda$ -MOS device is shown in Fig. 5. The measured threshold voltage of the testing n-channel MOS is 0.9 V at  $I_{DS} = 1 \mu A$ . From this, the fixed surface state charge density is estimated to be about  $2 \times 10^{11}/\text{cm}^2$ , which is consistent with the standard process of our laboratories.

The field effect mobility  $\mu_{FE}$  is also measured from the testing pattern. It is found that the effective mobility can be expressed by  $\mu_{FE} = 352.2(V_G - V_T)^{-0.45}$  for  $V_{GS} - V_T \geq 0.5$  V and  $564.2(V_{GS} - V_T)^{0.475}$  for  $V_G - V_T < 0.5$  V, which will give  $r = 0.45$ ,  $A = 352.2$  for  $V_{GS} - V_T \geq 0.5$  V, and  $r = -0.475$ ,

TABLE II  
LAYOUT PARAMETERS OF THE TESTING DEVICES

transistors parameters	Q1	Q2	Q3
	Geometrical Channel width ( $\mu\text{m}$ )	20	75
Geometrical Channel length ( $\mu\text{m}$ )	75	15	15
Effective Channel width ( $\mu\text{m}$ )	20	75	200
Effective Channel length ( $\mu\text{m}$ )	69.6	9.6	9.6

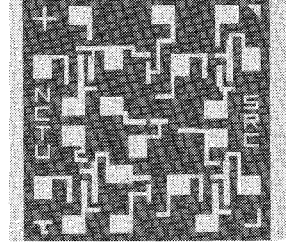


Fig. 4. Metallization pattern of the NELS-connected  $\Lambda$ -type negative resistance MOS device.

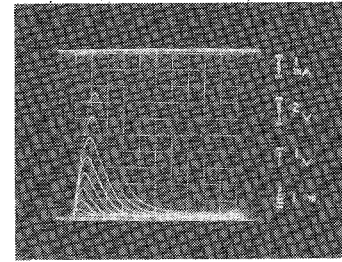


Fig. 5. Output characteristic of the fabricated device.

TABLE III  
SOME PHYSICAL CONSTANTS AND PARAMETERS USED FOR THE CALCULATION OF THE OUTPUT CHARACTERISTIC

$N_A$ ( $\text{cm}^{-3}$ )	$\approx 5 \times 10^{16}$	K	2.299
m	0.4	$G_r$	27.18
$N_{AS}$ ( $\text{cm}^{-3}$ )	$\approx 2 \times 10^{16}$	$\epsilon_o$ (F/cm)	$8.854 \times 10^{-14}$
$\phi_{fp}$ (volt)	0.365	$\epsilon_{ox}$	4
$t_{ox}$ ( $\text{\AA}$ )	1000	$\epsilon_s$	11.7

$A = 564.2$  for  $V_G - V_T < 0.5$  V. Some physical constants used are listed in Table III.

The calculated and the measured output characteristics for three different gate voltage  $V_{GG}$  are shown in Fig. 6. It is evident that more than 30 percent discrepancy appears in the negative resistance region. Although the boron surface segregation effect that comes from the impurity redistribution during the thermal growth of  $\text{SiO}_2$  is taken into consideration with segregation coefficient of  $m = 0.4$ , the slight discrepancy is still inevitable. The main reasons are due to assumptions of constant effective mobility in handling the current equation of the NELS inverter and the constant surface depletion charge density  $Q_B$  in the output current calculation.

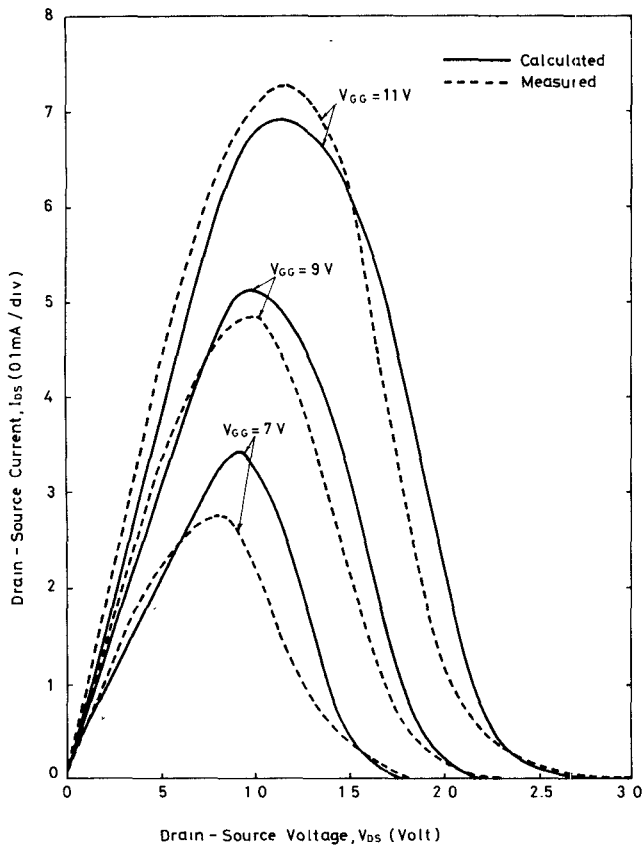


Fig. 6. Comparisons of theoretical and experimental output characteristics.

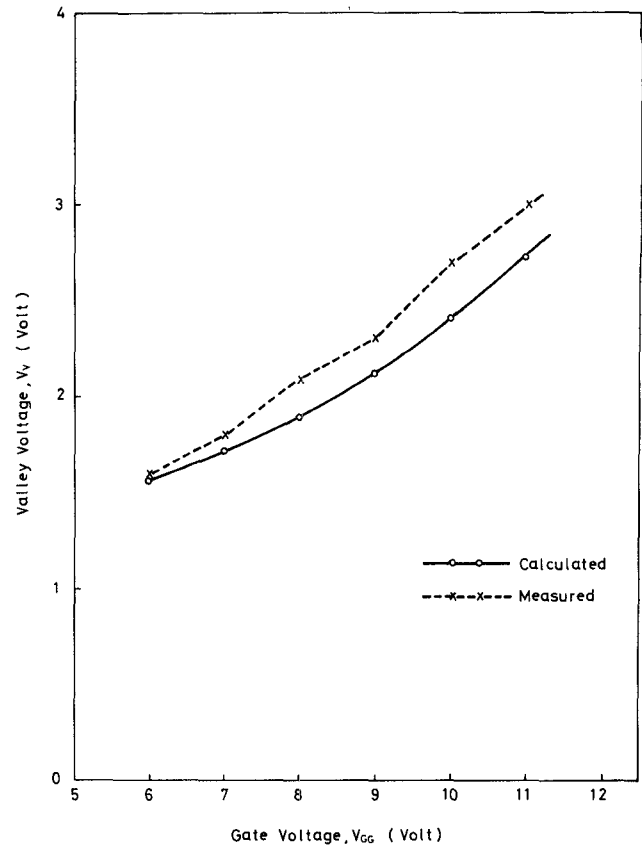


Fig. 8. Comparisons of theoretical and experimental valley voltage for different applied gate voltages  $V_{GG}$ .

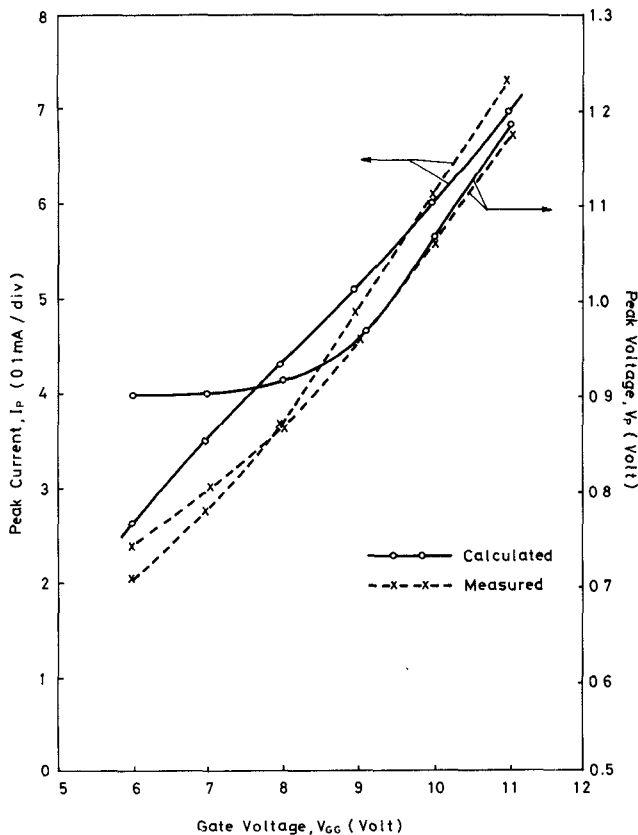


Fig. 7. Comparisons of theoretical and experimental peak voltage and peak current for different applied gate voltages  $V_{GG}$ .

From Fig. 7 it is found that there exists a good agreement between theoretical calculations and experimental results for the estimation of peak voltage and peak current at higher  $V_{GG}$ . The agreement becomes poor at lower  $V_{GG}$ , which is mainly attributed to the ambiguous definition of the threshold voltage and the effect of subthreshold leakage phenomena. The calculated and the measured valley voltages are shown in Fig. 8, where a good agreement is obtained under the assumption of valley current  $I_V = 1 \mu A$ .

Comparisons of the calculated and experimental negative differential resistance are shown in Fig. 9 for three different gate voltages. A discrepancy of less than 50 percent is observed over the 0.5 V negative resistance range. All the negative resistance values, which are determined from (23) and (24) in Section III, are related to  $V_{GS} = 3.5 \text{ V}, 3.25 \text{ V}, 3.0 \text{ V}, 2.75 \text{ V}, 2.5 \text{ V},$  and  $2.0 \text{ V}$ . The corresponding drain-to-source voltage  $V_{DS}$  for each  $V_{GS}$  are cited on the abscissae of the figure.

Fig. 10 shows the peak voltage variations in the temperature range from  $-55$  to  $125^\circ\text{C}$ . A theoretical coefficient of the threshold voltage variation with the temperature [8]; i.e.,  $dV_T/dT \approx 3.08 \times 10^{-3} \text{ V}/^\circ\text{C}$  is also given in the figure for comparison. The agreement between theory and the experimental result provides the fact that the peak voltage strongly depends on the threshold voltage of the device.

The peak current variations, in the temperature range from  $-55$  to  $125^\circ\text{C}$ , are shown in Fig. 11, where the reciprocal temperature scale is used. The mobility variation with

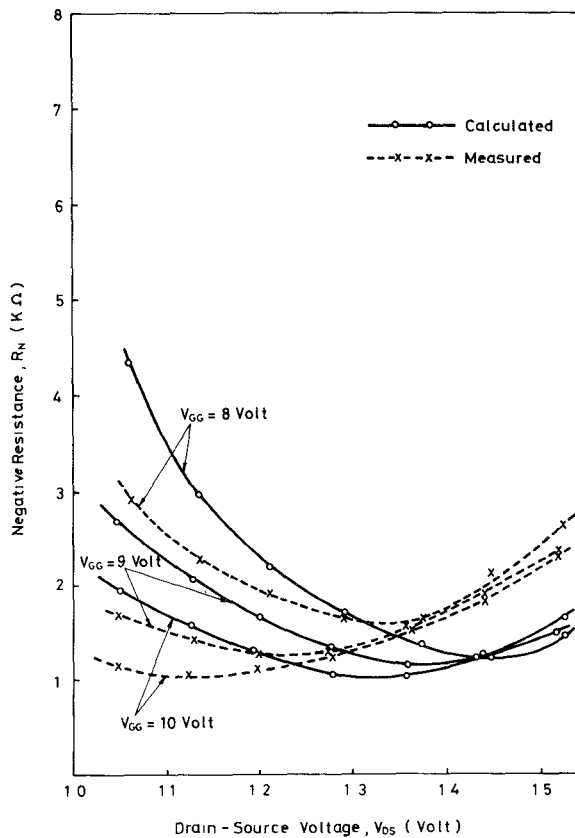


Fig. 9. Comparisons of theoretical and experimental negative resistance for  $V_{GG} = 8\text{ V}, 9\text{ V},$  and  $10\text{ V}.$

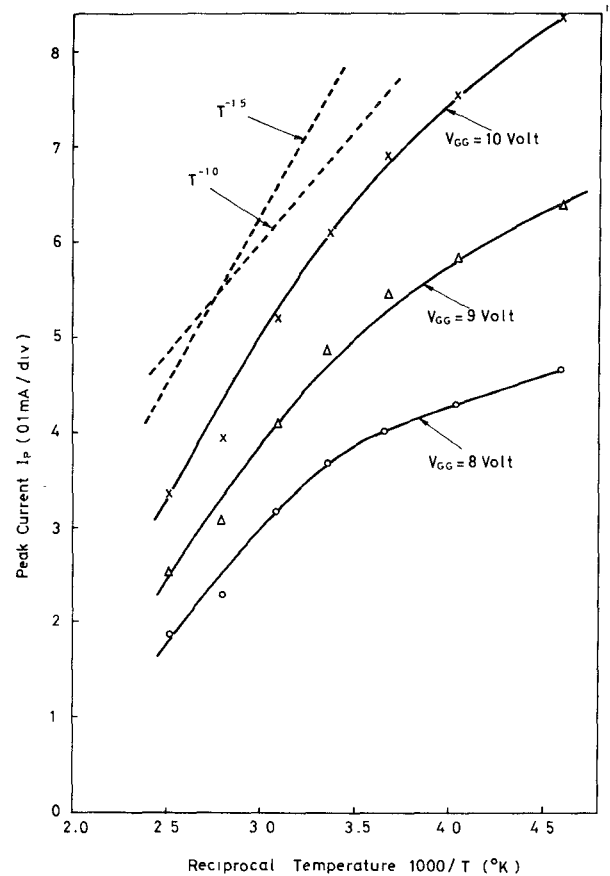


Fig. 11. Peak current variations with respect to temperature.

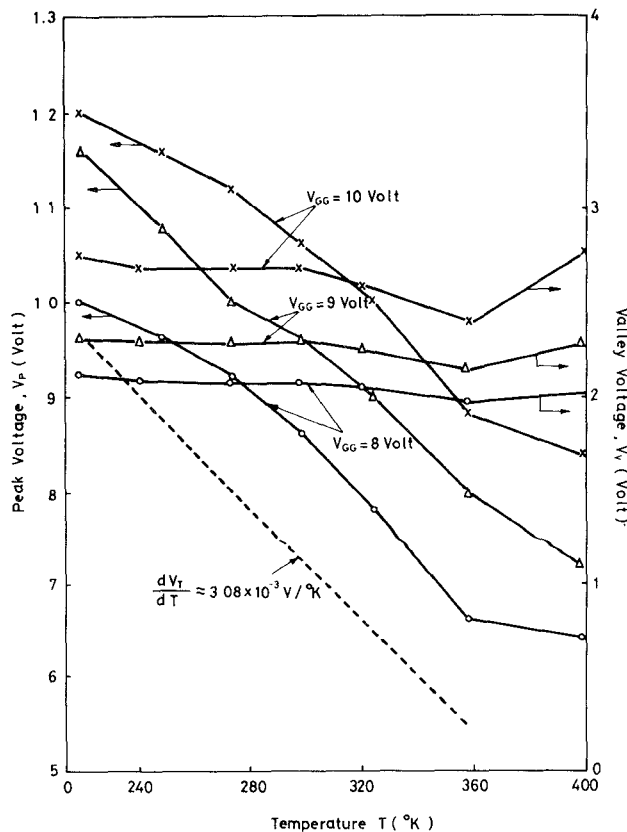


Fig. 10. Peak voltage and valley voltage variations with respect to temperature.

temperature plays an important role in determining the current-voltage characteristic of the MOSFET as a function of temperature. Two temperature functions of  $T^{-1}$  and  $T^{-1.5}$  are also given in the same figure as a guide to determine the variation of mobility with temperature, which is also justified.

The valley voltage is found more stable at this temperature range, as shown in Fig. 10, which is in quite good agreement with the theoretical prediction cited in (20), where the temperature effect is compensated for high  $V_{GG}$ .

### V. CONCLUSIONS

A NELS-connected three-terminal voltage controlled  $\Lambda$ -type negative resistance structure has been theoretically and experimentally analyzed. For a general description, a high ratio of zero drain voltage conductance of  $Q2$  to that of  $Q1$  is used; i.e.,  $G_r = 27.18$ , the observed negative resistance output swing is more than 1 V for different applied gate voltages, and the peak-to-valley current ratio are about several hundred with the definition of  $I_v = 1\ \mu\text{A}$ . Moreover, the negative resistance can be controlled from 1000 to 3000  $\Omega$  in the operating range of 0.5 V. Because of the substrate bias effect, the current handling capability of this NELS-connected structure is limited by using the conventional Al-gate MOSFET. An improvement can be carried out by using DMOS or VMOS fabrication technology. If three MOSFET's are replaced by three DMOS structures, the substrate and the source of transistor  $Q1$  can be connected together, and the substrate bias effect can be eliminated. This will lead to higher power

operation. Moreover, the inherent property of high-frequency response of DMOS and VMOS will also improve the frequency response of the present device.

In general, the voltage controlled  $\Lambda$ -type negative resistance MOSFET has several important features. First, it can be easily fabricated by the conventional planar MOS technology at low cost; second, it has a wide range of negative resistance, output swing, and high peak-to-valley current ratio; and third, it has good temperature stability.

#### ACKNOWLEDGMENT

The authors wish to thank Dr. D. D. Buss for his kind suggestions and English corrections, and all the technical staffs of the Semiconductor Research Center, National Chiao-Tung University, for their numerous contributions.

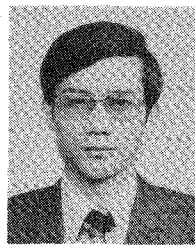
#### REFERENCES

- [1] H. Takagi and G. Kano, "Complementary JFET negative-resistance devices," *IEEE J. Solid-State Circuits*, vol. SC-10, pp. 509-515, Dec. 1975.
- [2] T. Mimura, "Voltage-controlled DNR in unijunction transistor structure," *IEEE Trans. Electron Devices*, vol. ED-21, pp. 604-605, Sept. 1974.
- [3] K. Lehovec and R. Zuleeg, "Negative resistance of a modified insulated-gate field-effect transistor," *Proc. IEEE*, vol. 62, pp. 1163-1165, Aug. 1974.
- [4] R. E. Thomas, W. Chin, and R. F. Haythornthwaite, "A surface-controlled negative impedance transistor," in *Proc. Int. Electron Device Meeting*, Washington, DC, 1973, Paper 17.2.
- [5] B. J. Baliga, D. E. Houston, and S. Krishna, "GAMBIT: Gate modulated bipolar transistor," *Solid-State Electron.*, vol. 18, pp. 937-941, 1975.
- [6] J. A. Porter, "JFET-transistor yields device with negative resistance," *IEEE Trans. Electron Devices*, vol. ED-23, pp. 1089-1099, Sept. 1976.
- [7] C.-Y. Wu and K.-N. Lai, "A new integrated voltage-controlled negative resistance device—the Lambda MOSFET," *Solid-State Electron.*, to be published.
- [8] S. M. Sze, *Physics of Semiconductor Devices*, 1969.



**Ching-Yuan Wu (M'72)** was born in I-Lan, Taiwan, Republic of China, on March 18, 1946. He received the B.S. degree in electrical engineering from the National Taiwan University, Taiwan, in 1968, and the M.S. and Ph.D. degrees in electrical sciences from the State University of New York at Stony Brook, in 1970 and 1972, respectively.

From 1972 to 1973 he was a Lecturer in the Department of Electrical Sciences, SUNY at Stony Brook. During the 1973-1975 academic years he was an Associate Professor in the Electronics Engineering Department, National Chiao-Tung University, Hsin-Chu, Republic of China. Since 1975 he has been a Professor in the Electronics Engineering Department, Director of Semiconductor Research Center, National Chiao-Tung University, Taiwan, Republic of China. He is also the Director of the Electronics Institute. He is the author of several books on electronics and circuits in Chinese, and over 30 technical papers and reports on semiconductor devices and circuits. His current research interests focus on chemical vapor deposition technique, new devices, and integrated-circuit technology.



**Khun-Nan Lai (S'75)** was born in Chaiyi, Taiwan, Republic of China, on May 25, 1950. He received the B.S. degree in electrophysics and the M.S. degree in electronic engineering from the National Chiao Tung University, Hsinchu, Taiwan, in 1972 and 1977, respectively.

Since 1977 he has been a Research Engineer at the Electronic Research Laboratory, Chung Shan Institute of Science and Technology. His current research focuses on the fabrication of infrared devices and the development of thin optical film technology.